Cell Calcium 56 (2014) 285–295

Contents lists available at ScienceDirect

Cell Calcium

journal homepage: www.elsevier.com/locate/ceca

Epigallocatechin-3-gallate elicits Ca^{2+} spike in MCF-7 breast cancer cells: Essential role of Cav3.2 channels

Elia Ranzato[a,1], Valeria Magnelli[a,1], Simona Martinotti[a], Zeina Waheed[b], Stuart M. Cain[b], Terrance P. Snutch[b], Carla Marchetti[c], Bruno Burlando[a,c,*]

[a] Dipartimento di Scienze e Innovazione Tecnologica, DiSIT, Università del Piemonte Orientale, viale T. Michel 11, 15121 Alessandria, Italy
[b] Michael Smith Laboratories, University of British Columbia, Rm 219 – 2185 East Mall, Vancouver, BC, Canada V6T 1Z4
[c] Istituto di Biofisica, Consiglio Nazionale delle Ricerche, via De Marini 6, 16149 Genova, Italy

ARTICLE INFO

Article history:
Received 19 April 2014
Received in revised form 29 May 2014
Accepted 1 September 2014
Available online 15 September 2014

Keywords:
$[Ca^{2+}]_i$ spike
Catalase
Cav3.1
Cav3.2
Confocal Ca^{2+} imaging
Kv1.1
Z944
T-type Ca^{2+} channels
Whole-cell voltage-clamp

ABSTRACT

We used MCF-7 human breast cancer cells that endogenously express Cav3.1 and Cav3.2 T-type Ca^{2+} channels toward a mechanistic study on the effect of EGCG on $[Ca^{2+}]_i$. Confocal Ca^{2+} imaging showed that EGCG induces a $[Ca^{2+}]_i$ spike which is due to extracellular Ca^{2+} entry and is sensitive to catalase and to low-specificity (mibefradil) and high-specificity (Z944) T-type Ca^{2+}channel blockers. siRNA knockdown of T-type Ca^{2+} channels indicated the involvement of Cav3.2 but not Cav3.1. Application of EGCG to HEK cells expressing either Cav3.2 or Cav3.1 induced enhancement of Cav3.2 and inhibition of Cav3.1 channel activity. Measurements of K^+ currents in MCF-7 cells showed a reversible, catalase-sensitive inhibitory effect of EGCG, while siRNA for the Kv1.1 K^+ channel induced a reduction of the EGCG $[Ca^{2+}]_i$ spike. siRNA for Cav3.2 reduced EGCG cytotoxicity to MCF-7 cells, as measured by calcein viability assay. Together, data suggest that EGCG promotes the activation of Cav3.2 channels through K^+ current inhibition leading to membrane depolarization, and in addition increases Cav3.2 currents. Cav3.2 channels are in part responsible for EGCG inhibition of MCF-7 viability, suggesting that deregulation of $[Ca^{2+}]_i$ by EGCG may be relevant in breast cancer treatment.

1. Introduction

Intracellular calcium ($[Ca^{2+}]_i$) plays a crucial role in cell survival, proliferation and growth through Ca^{2+} signaling and Ca^{2+}-dependent regulatory pathways [1,2]. Dysregulation of Ca^{2+} signaling or an aberrant rise in $[Ca^{2+}]_i$ will normally lead to cell death [3]. Due to the functional dependency of cell growth on $[Ca^{2+}]_i$, an essential role of Ca^{2+} is to be expected in the onset and development of cancer. This has been confirmed in a series of studies, showing the involvement of $[Ca^{2+}]_i$ in cancer initiation, tumor development, metastasis, invasion, and angiogenesis [4]. Such a body of evidence has raised interest in Ca^{2+} channels as potential targets for cancer therapy [5,6].

Epigallocathechin-3-gallate (EGCG) is a flavan-3-ol polyphenol that is abundantly present in green tea. This compound is known to exert chemopreventive activity by acting on various cellular targets in different cancer cell types [7,8]. Transformed cells are generally more sensitive to EGCG cytotoxicity than their normal counterparts, suggesting a possible use of the compound as a chemotherapeutic agent [9]. In addition, EGCG has shown a number of synergistic or additive interactions with different antitumor drugs, such as erlotinib, capecitabine, docetaxel and gemcitabine, and is therefore particularly interesting for the development of low-dosage combined therapies [10–14].

Following upon epidemiological evidence, considerable effort has been devoted to investigate the protective effects of EGCG against hormone related cancers, such as breast and prostate cancer [15]. EGCG has been extensively used on chemical-induced mammary carcinogenesis and breast cancer xenografts in rodents, while different clinical studies have also been carried out [16]. To explore the mechanism of action of EGCG, in vitro studies have assessed its cytotoxicity on breast cancer cell lines, which revealed an induction of cell cycle arrest and changes in intracellular signaling cascades that are strictly related to the onset of apoptosis [16].

In a few cases, EGCG has revealed the ability to interfere with $[Ca^{2+}]_i$ regulation [17–19]. Furthermore, our laboratory has previously shown that EGCG can induce a sustained $[Ca^{2+}]_i$ rise in

* Corresponding author. Tel.: +39 0131 360274; fax: +39 0131 360243.
E-mail address: burlando@unipmn.it (B. Burlando).
[1] These authors share equal contribution.

http://dx.doi.org/10.1016/j.ceca.2014.09.002
0143-4160/

mesothelioma cells through T-type Ca^{2+} channel opening [20]. T-type channels are low-voltage activated, Ca^{2+}-permeable ion channels whose principal, pore-forming subunits in vertebrates are Cav3.1, Cav3.2, and Cav3.3 [21]. They are functionally involved in the proliferation of non-cancerous cells, while their elevated, cell-cycle dependent expression has been reported in numerous types of tumors [22]. In some cases, it has been shown that targeting of T-type channels via siRNA knockdown, or by the use of non-specific blockers, such as mibefradil, has decreased cancer cell proliferation rates [23]. Hence, our previous finding that EGCG is able to interact with T-type Ca^{2+} channels opens up new opportunities for its possible use as an antitumor drug.

In this study, we have used confocal Ca^{2+} imaging and ionic current recordings to investigate EGCG-induced modulations of $[Ca^{2+}]_i$ in wildtype and siRNA-transfected MCF-7 human breast cancer cells [24]. These cells represent a suitable model for studying the role of Ca^{2+} channels in cancer growth because they express both Cav3.1 and Cav3.2 channels. [25,26]. The proliferation of MCF-7 cells is also inhibited by the T-type Ca^{2+} channel blockers NNC-55-0396 and mibefradil, as well as by siRNA-mediated knockdown of Cav3.1 and Cav3.2 channels [26,27]. Interestingly, Cav3.1 seems specifically involved in the repression of proliferation and the promotion of apoptosis in these cells [25].

Our results show that cell exposure to EGCG elicits a prominent spike in $[Ca^{2+}]_i$ due to T-type Ca^{2+} channel opening. This change may be due to multiple modulatory effects of EGCG, including the inhibition of K^+ currents together with an enhancement of Cav3.2 T-type channel activity.

2. Materials and methods

2.1. Reagents

Reagents were purchased from Sigma–Aldrich, unless otherwise indicated. The previously-identified, high-affinity, T-type specific Ca^{2+} channel antagonist Z944 was from the laboratory of one of the co-authors (TPS) [28].

2.2. Cell culture and viability assay

In vitro experiments were carried out on MCF-7 human breast cancer cells (ATCC). Cells were cultured in DMEM supplemented with 10% fetal bovine serum (FBS, Euroclone, Pero, Italy) and 1% antibiotic mixture (Sigma penicillin–streptomycin solution, P0781).

Cell viability was determined by the calcein assay, carried out using the lipophilic, nonfluorescent calcein-acetoxymethylester (calcein-AM). The probe penetrates cell membranes and is then cleaved by intracellular esterases, yielding the hydrophilic fluorescent dye. Cells were settled in 96-well plates for 24 h, and then treated with EGCG as specified. Thereafter, plates were washed with PBS, incubated for 30 min at 37 °C with a solution of 2.5 μM calcein-AM in PBS, and then read in a fluorescence reader (Infinite 200 Pro, Tecan, Wien) by using 485-nm excitation and 535-nm emission filters.

2.3. Measurements of free cytosolic Ca^{2+} concentration, $[Ca^{2+}]_i$

Cells were plated on glass-base dishes (Iwaki Glass, Inc., Tokyo, Japan), allowed to settle overnight, and then loaded with the cell-permeant, fluorescent calcium probe fluo-3/AM (20 mM) in the dark at 37 °C for 60 min. The loading buffer consisted of (mM) 10 HEPES, 140 NaCl, 10 glucose, 1 $MgCl_2$, 2 $CaCl_2$, 5 KCl, pH 7.4. For Ca^{2+}-free experiments, the ion was omitted from the loading buffer. After probe loading and washing, cells were examined through confocal time-lapse analysis, using a Zeiss LSM 510 confocal system interfaced with a Zeiss Axiovert 100 M microscope (Carl Zeiss Inc., Oberkochen, Germany). Excitation was obtained by the 488 nm line of an Ar laser, and emission was collected using a 505–550 bandpass filter. The laser power was reduced to 15% in order to lower probe bleaching. Confocal imaging was performed with a resolution of 512 × 512 pixels at 256 intensity values, with a framing rate of 1 frame/5 s. Several cells were viewed together through a 20× Plan-Neofluar Zeiss objective (0.5 NA). Fluo-3 fluorescence was measured in digitized images as the average value over defined contours of individual cells, using the ROI-mean tool of the Zeiss LSM 510 2.01 software. Fluo-3 calibration was achieved by the following equation [29]:

$$Ca^{2+} = \frac{K_d(F - F_{min})}{(F_{max} - F)}$$

where K_d = 400 nmol/L. F_{max} and F_{min} are maximum and minimum fluorescence intensities obtained by fluo 3 calibration after cell exposure to 500 μM A23187 for about 10 min, followed by addition of 20 mM EDTA.

2.4. Ionic current recording

2.4.1. MCF-7 cells

Membrane currents were measured in the whole-cell configuration of the patch-clamp method as previously described [30]. Twenty four hours before electrophysiological recordings, MCF-7 cells were plated on glass coverslips coated with Poly-D-Lysine (Sigma P7886). Whole-cell voltage-clamp currents were recorded by the Axon Axopatch 200A amplifier (Molecular Devices, Sunnyvale, CA, USA). Stimulation and acquisition were performed through a Digidata 1440 interface and Pclamp10 software (Molecular Devices). Cells were continuously superfused by gravity flow (10 mL/min) with an external solution containing (in mM) 140 NaCl, 5.4 KCl, 1.8 $CaCl_2$, 5 HEPES. The pH was adjusted to 7.35 with NaOH. Electrodes were pulled from Clark borosilicate glass capillaries and had a resistance of 4–8 MΩ when filled with an intracellular solution containing (in mM): 142 KCl, 10 HEPES, 2 EGTA, 2 $MgCl_2$, pH 7.3 with KOH. Currents were low-pass filtered at 2 kHz and digitized at 10 kHz. Capacitance transients were minimized by analog compensation and the value obtained was taken as an estimate of the cell capacitance. All current traces were further corrected for leak and residual transients by a P/4 protocol.

To measure Ca^{2+} currents, the external bath was changed to a solution containing 120 mM NaCl and 10 mM $CaCl_2$. In some experiments, we also used an external high-barium solution (in mM) 108 $BaCl_2$, 10 HEPES, pH 7.4 with Trizma base, and an internal filling solution devoted to block K^+ currents (in mM): 124 CsCl, 1 $CaCl_2$, 11 EGTA, 10 HEPES, 1 $MgCl_2$, pH 7.3 with CsOH. Change of solutions and application of modifiers, such as EGCG, was accomplished by gravity flow; control ion substitution experiments showed that the external bath was completely changed in 10 s, which was the maximal stimulation rate in these experiments. Depolarizing steps of 100 ms ranging between −50 and +20 mV for calcium currents and between −50 and +80 mV for potassium currents, were applied in 10 mV steps from a holding potential of −90 mV. The peak values were normalized by dividing by the cell membrane capacitance in order to obtain the *I–V* curve. Current traces were analyzed with Clampfit-10 (Molecular Device) and SigmaPlot software (Jandel Scientific, Erkrath, Germany).

2.4.2. HEK cells

HEK-tsa201 cells stably expressing human Cav3.1 or Cav3.2 T-type channels [31] were maintained and selected at 37 °C in a 5% CO_2 incubator, using Dulbecco's Modified Eagle's Medium (Invitrogen 12800-082) supplemented with 10% fetal bovine serum and

25 mg/mL Zeocin (Invitrogen R25001). Twenty four hours prior to electrophysiological recordings, the cells were seeded on glass coverslips coated with Poly-D-Lysine.

Whole-cell recordings were carried out at room temperature using an Axopatch 200B amplifier (Molecular Devices). Data were acquired using a Digidata 1322A (Molecular Devices) interface. Currents were low-pass filtered at 2 kHz and digitized at 10 kHz and series resistance was compensated by 70%.

Recording pipettes with a final resistance of 2.5–4 MΩ were filled with internal solution containing (in mM): 130 CH_3CsO_3S, 10 HEPES, 10 EGTA, 2 $MgCl_2$, 4 ATP-Mg, and 0.3 GTP-Na (pH 7.2; 290 mOsm). The external bath solution contained (in mM): 92 CsCl, 40 TEACl, 10 HEPES, 1 $MgCl_2$ and 2 $CaCl_2$ (pH 7.4; 310 mOsm). EGCG was dissolved directly into external recording solution and was applied with a BPS-8 perfusion system (ALA Scientific Instruments) at approximately 1 mL/min.

A series of 180 ms depolarizing steps of increasing amplitude were applied from a holding potential of −110 mV and the peak values were divided by the cell membrane capacitance in order to obtain the current density *I–V* curve. Data were fitted with a modified Boltzmann equation:

$$I_m = \frac{G_{max}(V - E_{rev})}{\{1 + \exp((V - V_{50})/k)\}}$$

Calcium currents elicited by repetitive voltage pulses of 120 ms applied every 5 s to a test value of −30 mV from a holding potential of −100 mV were recorded to examine the time course of the effect of 100 μM EGCG.

The time course for activation (τ_{act}) and inactivation (τ_{inact}) were analyzed by fitting current traces with a single exponential standard equation:

$$I = A \exp\left(\frac{-t}{\tau}\right)$$

where A is the amplitude of the current and τ is the time constant.

Activation curves were obtained by calculating conductance from the *I–V* curves and plotting the normalized conductance as a function of the membrane potential. The data was fitted with the Boltzmann equation:

$$\frac{G}{G_{max}} = A_2 + \frac{(A_1 - A_2)}{1 + \exp((V_m - V_{50})/k)}$$

where A_1 is minimum normalized conductance, A_2 is maximum normalized conductance, V_m is the test potential, V_{50} is the half-activation potential, and k value the slope of the activation curve (slope constant).

Steady-state inactivation was studied with a voltage protocol consisting of 90 ms test pulses at −30 mV preceded by a 2 s conditioning pre-pulse ranging from −120 to −10 mV. The current amplitude recorded during each test pulse was normalized to the maximum value, with prepulse at −120 mV, and plotted as a function of the pre-pulse potential. The data was fitted with the Boltzmann equation:

$$\frac{I}{I_{max}} = A_2 + \frac{(A_1 - A_2)}{1 + \exp((V_m - V_{50})/k)}$$

where A_1 is minimum normalized current, A_2 is the maximum normalized current, V_m is the test potential, V_{50} is the half-inactivation potential and k reflects the slope of the inactivation curve (slope constant). Current traces were analyzed with Clampfit and Origin software.

Table 1
Sequences of primers used for qRT-PCR.

GAPDH	Forward	5′-AATCCCATCACCATCTTCCA-3′
	Reverse	5′-TGGACTCCACGACGTACTCA-3′
β-Actin	Forward	5′-TCCCTGGAGAAGAGCTACGA-3′
	Reverse	5′-AGCACTGTGTTGGCGTACAG-3′
CACNA1G	Forward	5′-GGACTTCTCTTCATGTTGTTG-3′
	Reverse	5′-GTCCTTCATAATGCCATTCC-3′
CACNA1H	Forward	5′-TGCTACGAAGAGCTGCTGAA-3′
	Reverse	5′-GCCATGGCTGAAATGGTAGT-3′

GAPDH: glyceraldehyde-3-phosphate dehydrogenase; CACNA1G: Cav3.1 T-type Ca^{2+} channel; CACNA1H: Cav3.2 T-type Ca^{2+} channel.

2.5. Quantitative reverse transcriptase PCR (qRT-PCR) and RNA interference (siRNA)

Cells were settled in multiwell plates for 24 h and then subjected to the indicated experimental conditions. NucleoSpin RNA II Kit (Macherey-Nagel, Düren, Germany) was then used to purify total RNA. Complementary DNA was synthesized from RNA using the Transcriptor First Strand cDNA Synthesis Kit (Roche Diagnostics GmbH, Penzberg, Germany). qRT-PCR was carried out using Power Sybr Green Mastermix (Ambion Austin, TX) and KiCqStart® SYBR® Green Primers (Sigma–Aldrich, Table 1) in a CFX384 Real-Time PCR Detection System (Bio-Rad Laboratories, Hercules, CA). For the KCNA1 gene, coding for the Kv1.1 K^+ channel, the Qiagen QuantiTect® primer assay (Cat. No: QT01195733) was used. Gene expression was calculated using the ΔΔCt method.

RNA interference was obtained by transfecting cells with 5 μM siRNA oligonucleotides (Sigma–Aldrich, Table 2) or with equimolar scramble siRNA by using the N-ter Nanoparticle siRNA Transfection System (Sigma–Aldrich). Scramble siRNA was obtained using commercial non-targeting siRNA (MISSION siRNA Universal Negative Control). Cells were harvested at 24 or 72 h after transfection and used for the indicated experiments.

2.6. Western blotting

Amounts of 100 μg of protein from cell lysates were subjected to SDS PAGE (12% gel), blotted to nitrocellulose membrane and probed with a primary monoclonal antibody against the Cav3.2 calcium channel (clone S55-10, cat. no. 13704, Cayman Chemicals, Cabru, Milan, Italy, dilution 1:400) followed by a horseradish peroxidase-conjugated secondary antibody (Bethyl Laboratories, Montgomery, TX, USA; dilution 1:1000). The membrane was then developed using an ECL kit (Millipore, Billerica, MA, USA), acquired by ChemiDoc XRS and digitized with Quantity One Imaging system (Bio-Rad). Equal loading of wells was confirmed using anti-actin antibody (Santa Cruz Biotechnology, Santa Cruz, CA, USA).

2.7. Statistics

Data were analyzed with the R package, version 3.0.1 (The R Foundation for Statistical Computing, http://www.r-project.org/foundation/). Statistical comparisons were carried out by *t* test, using Bonferroni's correction for multiple comparisons.

Table 2
Sequences of siRNA oligonucleotides.

Double strand	CACNA1G	Sense	5′-CAGUCUUUCUGGCUGAAAU-3′
		Antisense	5′-AUUUCAGCCAGAAAGACUG-3′
	CACNA1H	Sense	5′-CUGACUAAUGCUCUGGAGA-3′
		Antisense	5′-UCUCCAGAGCAUUAGUCAG-3′
Single strand	KCNA1		5′-AAGCTACTGACCGATGTTTAA-3′

KCNA1: Kv1.1 K^+ channel; other gene name codes as in Table 1.

Values of IC50 and their 95% confidence intervals (95% CI) were determined using a downhill sigmoidal dose–response curve developed by CSIRO, Australia [32]:

$$y = \frac{T}{1 + \exp(-S(\log D - \log IC_{50}))}$$

where T = top, S = Hill's slope (negative for a downhill curve), D = EGCG concentration in μmoles/L. Statistical comparisons between IC_{50} values were based on overlapping or non-overlapping 95% CI.

3. Results

3.1. EGCG induces a $[Ca^{2+}]_i$ spike in MCF-7 cells

Confocal imaging of fluo 3-loaded MCF-7 cells exposed to EGCG revealed the occurrence of a single, large $[Ca^{2+}]_i$ spike. The spike started a few seconds after exposure, reached a peak within 20–30 s, and recovered to baseline in approximately 100–200 s (Fig. 1A and B). The size of the spike showed variability among cells, spanning a range of 500–1100 nM.

3.2. The EGCG-induced $[Ca^{2+}]_i$ spike depends on a redox mechanism and involves T-type Ca^{2+} channels

The observed effect on $[Ca^{2+}]_i$ suggests the involvement of Ca^{2+} regulatory systems and a series of tests was designed in order to determine the underlying mechanism. The effect of increasing EGCG concentrations showed that the spike was dose-dependent (Fig. 1C). Additionally, after EGCG treatment, the spike was absent in the absence of external Ca^{2+} in the cell medium, or in the presence of mibefradil, a T-type channel blocker of low specificity, or of 10 nM Z944, a highly selective T-type channel blocker [28]. As shown in Fig. 1D, the traces of average $[Ca^{2+}]_i$ variations with time under these conditions are almost overlapped and flat. These data indicate that the EGCG-mediated spike is due to the entry of external Ca^{2+} via activation of T-type channels.

We have previously shown that EGCG induces a redox-dependent $[Ca^{2+}]_i$ rise in malignant mesothelioma cells through the release of H_2O_2 in the cell medium [20]. Therefore, we used confocal imaging to monitor $[Ca^{2+}]_i$ variations in MCF-7 cells exposed to EGCG in the presence of 500 U/mL catalase. Under these conditions, the EGCG-mediated $[Ca^{2+}]_i$ spike was completely abolished. Moreover, the sulfhydryl reagent DTNB (200 μM) induced a $[Ca^{2+}]_i$ spike similar to that obtained with EGCG (Fig. 1E).

3.3. The EGCG effect is mediated by the Cav3.2 T-type channel

Further evidence for the involvement of T-type Ca^{2+} channels was investigated using siRNA knockdown targeting the human CACNA1G and CACNA1H genes, which encode for the Cav3.1 and Cav3.2 T-type Ca^{2+} channels, respectively. We first confirmed the expression of the Cav3.1 and Cav3.2 isoforms in MCF-7 cell clonal line using qRT-PCR (Fig. 2A). Thereafter, gene knockdown of Cav3.1 or Cav3.2 was performed by siRNA transfection and confirmed by both qRT-PCR and Western blotting (Fig. 2B and C). Confocal imaging revealed that the EGCG-induced $[Ca^{2+}]_i$ spike was absent following Cav3.2 knockdown, whereas Cav3.1 knockdown did not modify the EGCG effect. The $[Ca^{2+}]_i$ spike was also retained in cells treated with scramble siRNA (Fig. 2D).

3.4. EGCG differently modulates the activities of Cav3.1 and Cav3.2 channels

Calcium currents in MCF-7 cells were recorded in patch-clamp whole-cell configuration from a holding potential of −90 mV and 100 ms voltage steps ranging between −50 and +20 mV (in 10 mV increments). Calcium currents were successfully recorded in only 10% of the cells, showed peak values averaging ≤20 pA, and were sensitive to block by Ni^{2+} (Fig. 3A). Further trials with high (108 mM) Ba^{2+} external solution and Cs-based pipette solution (see Section 2) did not reveal larger calcium currents. Current–voltage (*I–V*) relationships, recorded in 10 mM external Ca^{2+} and normalized to cell capacitance, showed voltage-dependence properties typical of low threshold T-type Ca^{2+} channels, peaking between −20 and −10 mV (Fig. 3B).

The finding of such small Ca^{2+} currents in MCF-7 cells is not inconsistent with our confocal microscopy data, since it is known that small Ca^{2+} currents that are difficult to assess using electrophysiological means can however still generate sufficiently large $[Ca^{2+}]_i$ variations to be assessed with Ca^{2+} imaging using fluorescent probes [33,34].

As the Ca^{2+} currents were small and sporadic in MCF-7 cells, the effect of EGCG was further investigated in stably transfected HEK cells expressing human isoforms of either Cav3.1 or Cav3.2 (Fig. 3C–J). Current traces (Fig. 3C–D) were recorded at −30 mV from a holding potential of −110 mV. Bath application of 100 μM EGCG resulted in about 50% reduction of Ca^{2+} current through Cav3.1 channels (n = 5; Fig. 3C) and a marked increase of currents through Cav3.2 channels (n = 14; Fig. 3D). Fig. 3E shows the average percentage change caused by 100 μM EGCG in peak T-type current in the different channel types, while Fig. 3F shows the dose dependence of EGCG-mediated potentiation of Cav3.2 currents. A dose of 100 μM caused the maximum potentiation (169.6 ± 43.0%), while 1 mM EGCG induced an inhibition of Cav3.2 currents. This observation suggests that higher doses of EGCG trigger inhibitory effects on Cav3.2 channels, justifying the use of 100 μM.

Fig. 3G shows the effect of EGCG on Cav3.2 current density as a function of membrane potential. EGCG (100 μM) caused not only a marked increase in current density, but also a leftward shift in the Cav3.2 *I–V* relationship. The activation curve (Fig. 3H) shows that this shift is a result of a lowering of the threshold activation voltage and a shift of V_{50} in the hyperpolarizing direction, from −38.1 ± 2.5 mV in control to −49.6 ± 6.6 mV in EGCG-treated cells ($p < 0.01$). Furthermore, a decrease is also observed in the activation slope constant (from k = 7.8 ± 1.1 in control to k = 5.3 ± 1.3 mV in the presence of 100 μM EGCG; $p < 0.05$). On the contrary, EGCG did not have significant effects on steady-state inactivation or on activation and inactivation kinetics of control versus EGCG-treated Cav3.2 currents (Fig. 3H–J).

3.5. K^+ currents have a role in the EGCG-induced $[Ca^{2+}]_i$ spike

MCF-7 cell exposure to elevated extracellular K^+ resulted in a sustained increase of $[Ca^{2+}]_i$ that was blocked by mibefradil in line with the activation of voltage-gated Ca^{2+} channels, presumably via depolarization of the membrane potential (Fig. 4A). We therefore explored the possibility that EGCG may induce K^+ current inhibition, leading to influx of Ca^{2+}. Measurements of K^+ currents showed a partial, reversible inhibition by EGCG (Fig. 4B and C), ranging at about 70–80% in the interval −20 to −10 mV (Fig. 4C, inset). Moreover, in the presence of catalase the EGCG-dependent inhibition of K^+ currents was abolished, indicating that EGCG may act by a redox mechanism (Fig. 4D). These data suggest that, by reducing K^+ currents, EGCG causes membrane depolarization that in turn activates T-type Ca^{2+} channels.

Thereafter, we evaluated the consequences of K^+ channel knockdown on the $[Ca^{2+}]_i$ modulation exerted by EGCG. Previous studies have reported the expression of Kv1.1 K^+ channels in MCF-7 cells and their role in cell proliferation [35]. In our study, the expression of Kv1.1 in MCF-7 cells was confirmed by qRT-PCR (Fig. 5A). This technique also revealed a reduction of Kv1.1 expression in cells

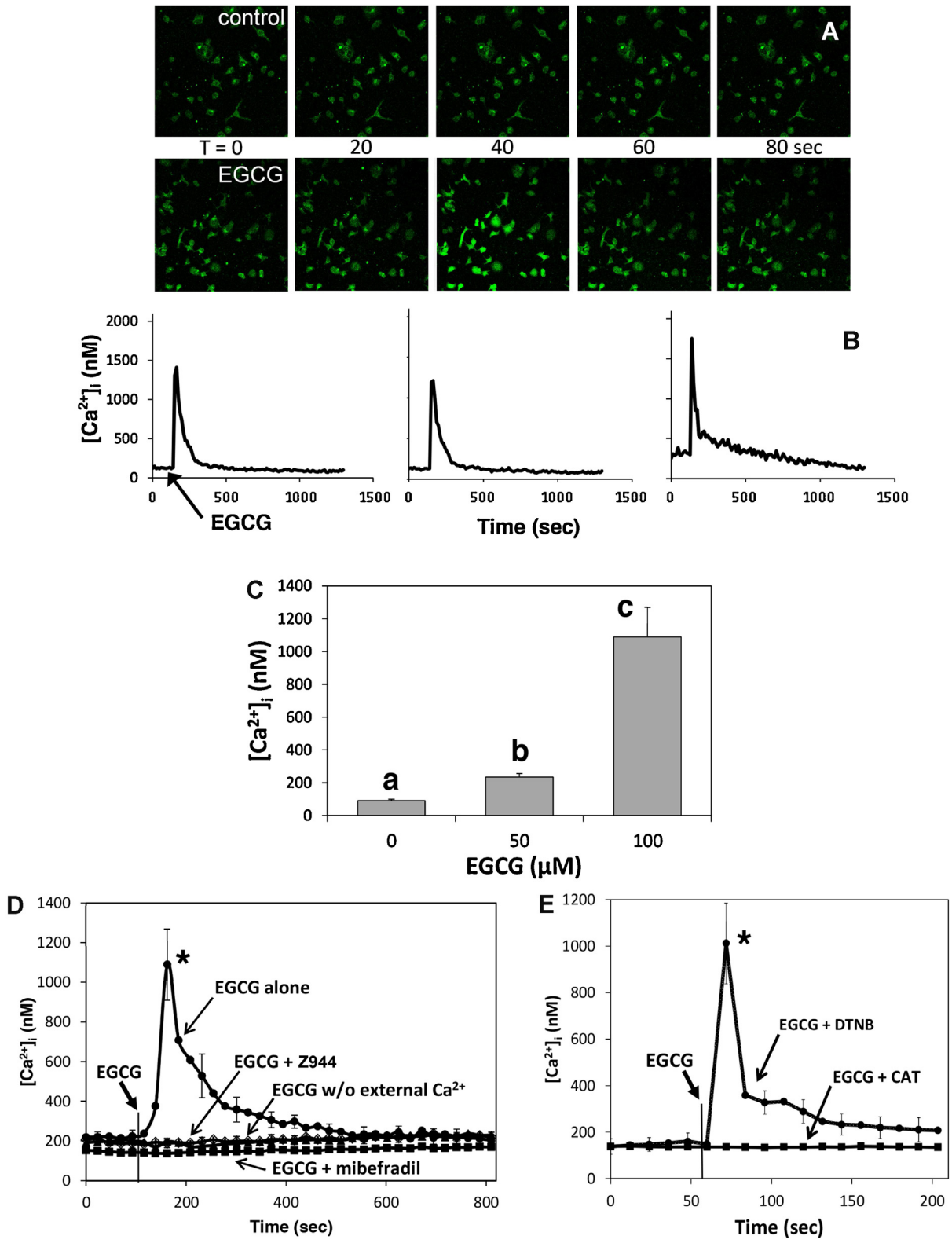

Fig. 1. Confocal Ca^{2+} imaging of MCF-7 cells loaded with the fluo-3 probe and exposed to EGCG (see Section 2). (A) Time lapse confocal images (field size, 450 μm × 450 μm) showing variation of intracellular fluo-3 fluorescence in different cells after exposure to 100 μM EGCG. (B) Representative traces of $[Ca^{2+}]_i$ variations recorded at 5-s intervals in individual cells, showing that exposure to 100 μM EGCG induces a single $[Ca^{2+}]_i$ spike lasting about 100–200 s, followed by complete baseline recovery. (C) Measurements of Ca^{2+} spikes elicited by cell exposure to increasing EGCG concentrations. Data are means ± s.e.m. of $[Ca^{2+}]_i$ measured by confocal imaging at peak maxima. Number of cells: 0 μM EGCG: a total of 43 cells from 3 different experiments; 50 μM EGCG: 22 cells from 2 exp.; 100 μM EGCG: 40 cells from 2 exp. Different letters on bars indicate statistical differences determined by pairwise *t* test with Bonferroni's correction ($p < 0.01$). (D) $[Ca^{2+}]_i$ variations recorded at 25-s intervals, showing Ca^{2+} spike after exposure to 100 μM EGCG alone, and in contrast, complete spike disappearance in Ca^{2+}-free medium, or in the presence of 5 μM mibefradil or 10 nM Z944 (20 min preincubation). Data are means ± s.e.m. of $[Ca^{2+}]_i$ recorded in different cells. EGCG alone: 40 cells from 3 exp.; EGCG w/o external Ca^{2+}: 19 cells from 2 exp.; EGCG + mibefradil: 65 cells from 4 exp; EGCG + Z944: 47 cells from 4 exp. *$p < 0.001$, *t*-test with Bonferroni's correction. (E) $[Ca^{2+}]_i$ variations recorded as in D, showing Ca^{2+} spike after exposure to 200 μM DTNB, and in contrast, absence of spike in cells exposed to EGCG in the presence of 500 u/mL catalase (CAT). Data and statistics as in D. EGCG + CAT: 79 cells from 3 exp.; DTNB: 24 cells from 3 exp.

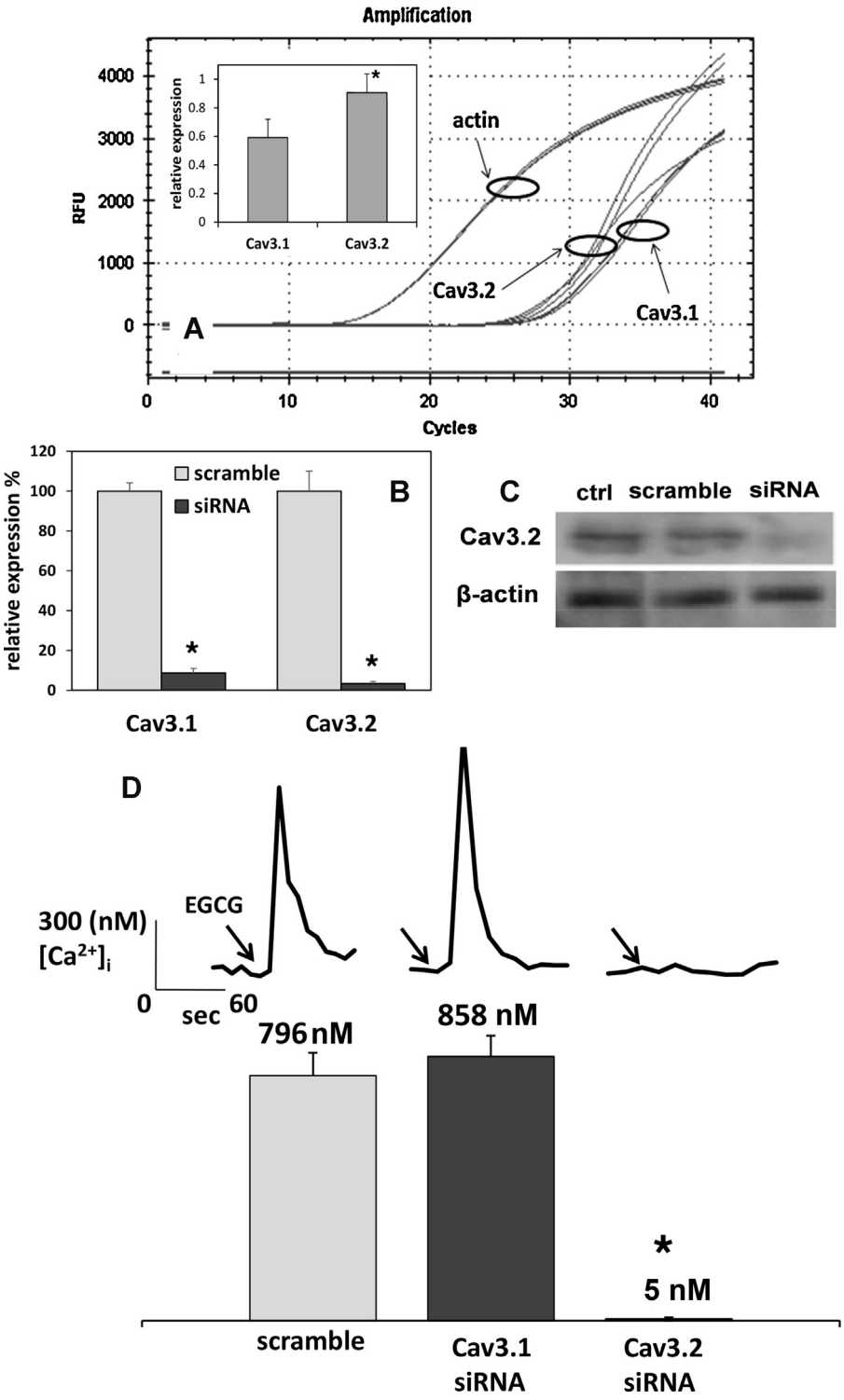

Fig. 2. Role of T-type Ca^{2+} channels in $[Ca^{2+}]_i$ variations induced by EGCG. (A) Expression of the Cav3.1 and Cav3.2 genes in MCF-7 cells, determined by qRT-PCR (see Section 2). Amplification curves from qRT-PCR analysis of control cells show distinct, tightly clustered readouts ($n = 3$) for housekeeping actin, Cav3.1, and Cav3.2 genes. The inset shows the relative expression of mRNA. $^*p < 0.05$. (B) Quantification by qRT-PCR of Cav3.1 and Cav3.2 mRNA in cells subjected to scramble or specific siRNA. Data are means ± sd of percent relative expressions ($n = 3$, $^*p < 0.001$). (C) Western blot of cell lysates showing quite detectable expression of the Cav3.2 peptide in control and scramble siRNA cells, and in contrast, strongly reduced expression after Cav3.2 siRNA. β-Actin bands are shown as loading control. (D) Representative traces show $[Ca^{2+}]_i$ spikes elicited by EGCG in cells transfected with scramble (left), Cav3.1 (center), or Cav3.2 (right) siRNA. Bars represent means ± s.e.m. of delta (peak-basal) $[Ca^{2+}]_i$ recorded in single cells. Scramble siRNA: 25 cells from 3 exp.; Cav3.1 siRNA: 30 cells from 3 exp.; Cav3.2 siRNA: 30 cells from 3 exp. $^*p < 0.001$, *t* test with Bonferroni's correction.

transfected with Kv1.1-specific siRNA (Fig. 5B). Confocal imaging of fluo 3-loaded cells showed an average reduction of about 50% of the EGCG-induced $[Ca^{2+}]_i$ spike in Kv1.1 siRNA-treated cells with respect to scramble siRNA-treated cells (Fig. 5C).

3.6. Cav3.2 has a role in EGCG-induced cytotoxicity to MCF-7cells

EGCG is known to produce cytotoxic effects on various cancer cell lines, including MCF-7 cells [36]. In order to investigate a

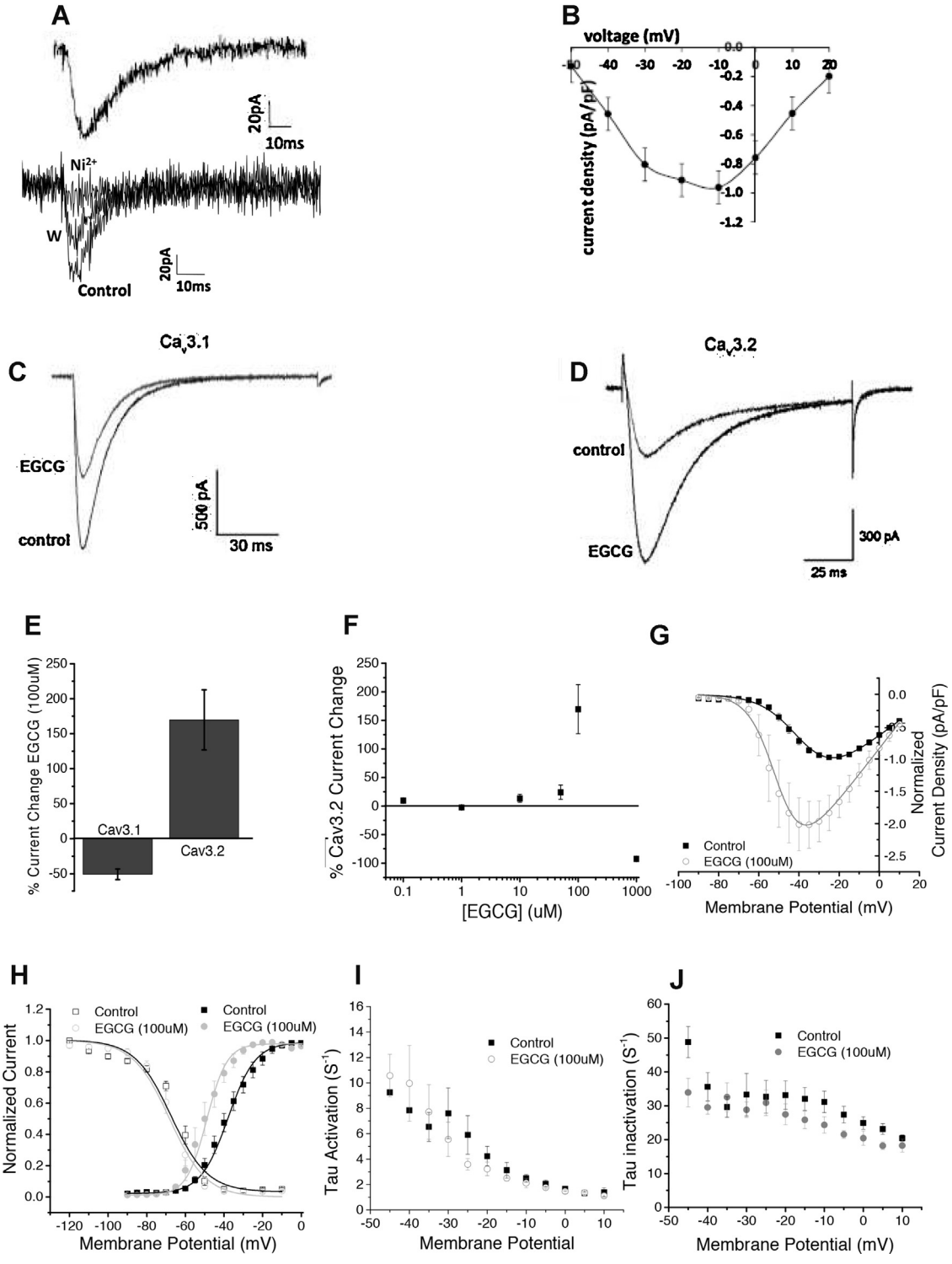

Fig. 3. Modulation of voltage-dependent T-type Ca^{2+} channel activity by EGCG. (A) Representative traces of inward Ca^{2+} currents recorded in MCF-7 cells at $V = -10$, 100 ms pulse. One of the control traces is overimposed with current recordings in the presence of 40 μM Ni^{2+} and after washout. (B) Averaged Ca^{2+} current density plotted as a function of membrane potential. Data were obtained in patch-clamp experiments on MCF-7 cells under control conditions (see Section 2). (C and D) Representative current traces from Cav3.1 (C) and Cav3.2 (D) T-type calcium channels exogenously expressed in HEK cells (see Section 2). Data show that 100 μM EGCG inhibits Cav3.1 current (C) and increases Cav3.2 current (D). (E) Mean percentage change in peak current induced by a depolarizing voltage step from −110 mV to −30 mV for Cav3.1 ($n = 5$) and Cav3.2 ($n = 14$) T-type Ca^{2+} channel isoforms expressed in HEK cells. (F) Concentration-response curve for the effect of EGCG on Cav3.2 currents at 0.1 μM ($n = 3$), 1 μM ($n = 4$), 10 μM ($n = 4$), 50 μM ($n = 3$), 100 μM ($n = 14$) and 1 mM ($n = 5$). (G) Cav3.2 current density as a function of voltage in HEK cells, in control and in the presence of EGCG 100 μM ($n = 6$ for both). (H) Voltage dependence of activation ($n = 6$) and steady-state inactivation ($n = 6$) curves for control versus EGCG-treated Cav3.2 currents. (I and J) Kinetics of activation (I) and inactivation (J) for control versus 100 μM EGCG-treated Cav3.2 currents ($n = 6$ for both).

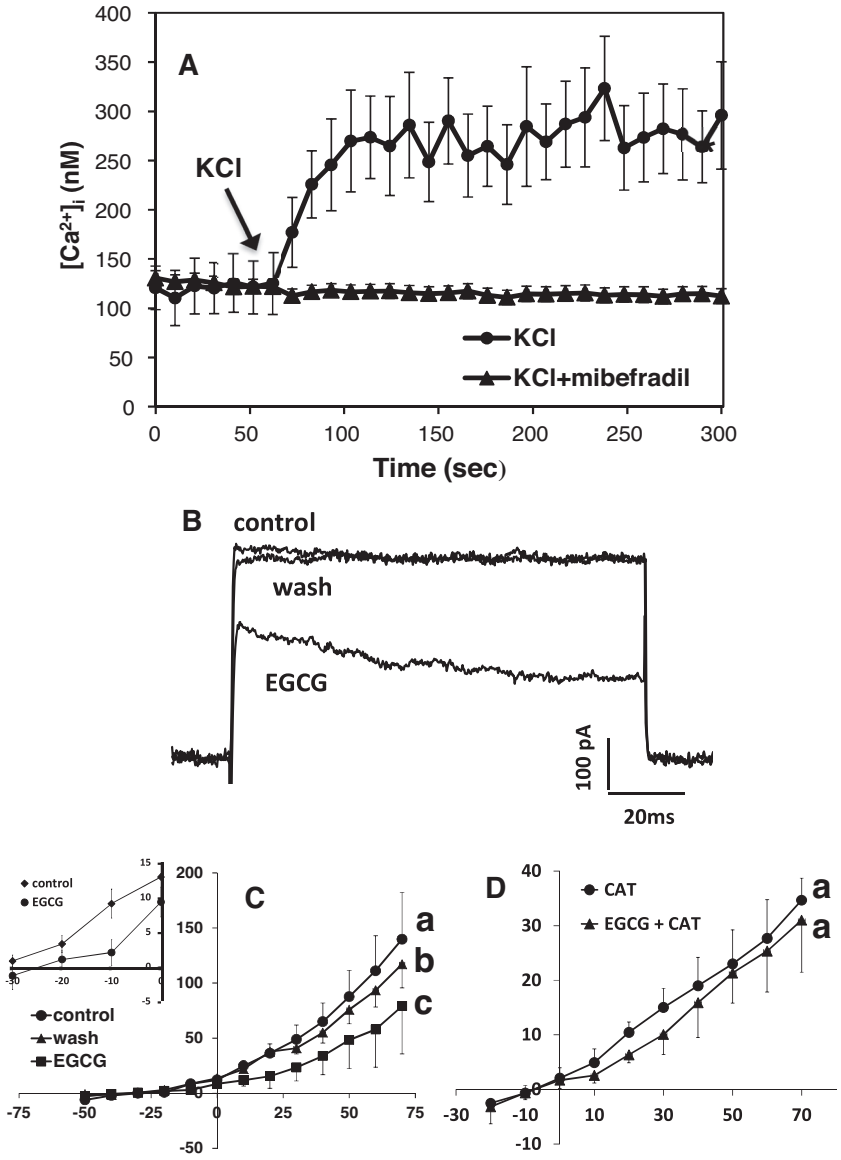

Fig. 4. (A) $[Ca^{2+}]_i$ variations recorded at 10-s intervals in individual MCF-7 cells, showing sustained $[Ca^{2+}]_i$ rise after exposure to 50 μM KCl, and disappearance of the effect in the presence of 5 μM mibefradil. Data are means ± s.e.m. of $[Ca^{2+}]_i$ recorded in different cells. Number of cells: 49 from 3 exp. (KCl alone), 43 from 3 exp. (KCl + mibefradil). (B) Whole-cell K^+ current traces recorded from a representative MCF-7 cell upon a step depolarization of 100 ms to +70 mV from a holding potential of −90 mV. Traces show control trace in standard external and internal solutions, trace recorded after exposure to 100 μM EGCG, and upon wash out. (C) Current-to-voltage relationship averaged in $n = 9$ cells. Currents were recorded upon application of 100 ms voltage steps ranging between −50 and +70 mV from a holding potential of −90 mV. The inset shows detail of data between −40 and 0 mV from control and EGCG-exposed cells. Data are means ± sd; different letters indicate statistical differences as in Fig. 1C ($p < 0.01$), t test with Bonferroni's correction; EGCG = 100 μM. (D) Current-to-voltage relationship averaged on $n = 3$ cells. Data and statistics as in C.

possible role of T-type Ca^+ channels in the EGCG-mediated cytotoxicity of MCF-7 cells we determined dose–response curves by using the cell viability calcein assay for 24 h. We first evaluated EGCG effects on wildtype MCF-7 cells, finding an $IC_{50} = 19$ μM (95% CI = 17–21). Thereafter, we applied the calcein assay to cells transfected with Cav3.2-specific siRNA or scramble siRNA, observing a significant increase of the EGCG IC_{50} in cells transfected with specific siRNA with respect to scramble siRNA (Fig. 6). These data indicate a lowering of EGCG cytotoxicity after Cav3.2 gene silencing, suggesting that this channel contributes to the cytotoxic mechanism of action of EGCG.

4. Discussion

The role of low voltage-activated T-type Ca^{2+} channels in cell proliferation has been a topic of considerable interest. These channels exhibit higher expression density in growing cells and increased T-type currents are essential for cell cycle progression [22,23]. Of further note, an enhanced expression of T-type Ca^{2+} channels is found in cancer cells, giving rise to interest in their possible use as therapy targets [26,37].

Our previous study focused on Cav3.2-dependent Ca^{2+} dynamics induced by EGCG in malignant mesothelioma [20]. In the present study, we examined MCF-7 human breast cancer cells as a more suitable model to study the mechanism of action of EGCG on $[Ca^{2+}]_i$ in cancer. The activity of Ca^{2+} channels and the effects of EGCG treatments on MCF-7 cells have been explored in separate studies [16,26] but the specific action of EGCG on the Ca^{2+} channel isoforms expressed in these cells had yet to be investigated.

The $[Ca^{2+}]_i$ spikes we observed are the first evidence of a transient Ca^{2+} signal induced by EGCG in cancer cells. A combination of confocal imaging, whole cell current recording and

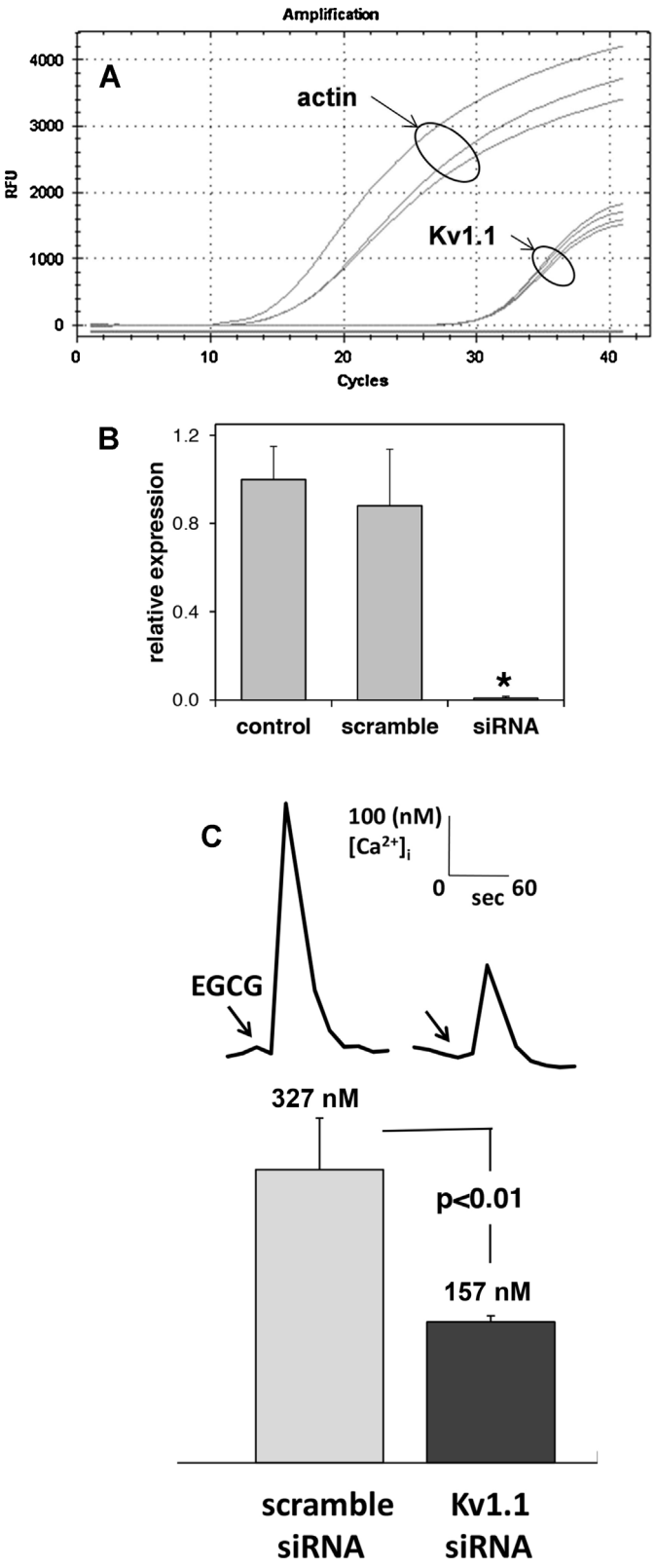

Fig. 5. Role of Kv1.1 potassium channel in the modulation of $[Ca^{2+}]_i$ induced by EGCG. (A) Amplification curves from qRT-PCR analysis of control MCF-7 cells show tightly clustered readouts ($n = 3$) for actin and Kv1.1. (B) Quantification of Kv1.1 mRNA in control cells or in cells subjected to scramble or Kv1.1 siRNA for 24 h. Data are mean ± sd of relative expressions ($n = 3$, $^*p < 0.001$, Bonferroni's test). (C) $[Ca^{2+}]_i$ variations recorded at 12-s intervals in cells transfected with scramble (left) or Kv1.1 (right) siRNA, and then exposed to 100 μM EGCG. Representative traces show $[Ca^{2+}]_i$ spikes elicited by EGCG in single cells. Bars represent means ± s.e.m. of delta $[Ca^{2+}]_i$ (peak-basal) recorded in single cells. Number of cells: 54 cells from 4 exp. (scramble siRNA), 45 cells from 3 exp. (Kv1.1 siRNA).

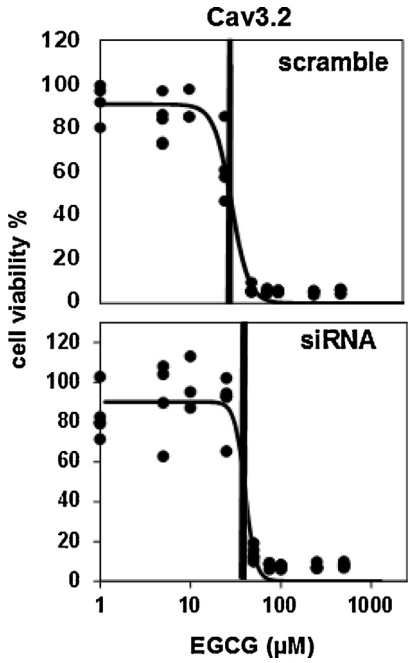

Fig. 6. Dose–response curves determined by the calcein cell viability assay (see Section 2) in MCF-7 cells transfected with scramble or Cav3.2 siRNA for 24 h, and then exposed to increasing EGCG concentrations (1, 5, 10, 25, 50, 75, 100, 250, 500 μM). The graphs show the following: (i) single readouts deriving from two independent experiments, each with $n = 4$; (ii) regression line obtained by fitting a downhill logistic curve (see Section 2); (iii) IC_{50} (vertical lines). The EGCG IC_{50} was of 20 μM (95% CI = 14–30) in scramble siRNA cells, and of 40 μM (34–48) in Cav3.2 siRNA cells ($p < 0.05$).

pharmacological analyses indicates that the $[Ca^{2+}]_i$ spike is driven by a redox process, is dependent on Ca^{2+} entry, and involves T-type Ca^{2+} channels.

Further evidence underlining the involvement of T-type Ca^{2+} channels was achieved by siRNA-mediated knockdown, which indicated a predominant role for Cav3.2 channels, whereas the involvement of Cav3.1 channels appeared negligible. In support of this, qRT-PCR data revealed that Cav3.2 mRNA expression is higher than that of Cav3.1 in MCF-7 cells. Furthermore, Cav3.1 and Cav3.2 Ca^{2+} currents exogenously expressed in HEK cells demonstrated opposing effects of 100 μM EGCG on the two channel subtypes, with Cav3.2 potentiation and Cav3.1 inhibition. Even though these latter data were collected on a different experimental model, they are consistent with confocal evaluation of $[Ca^{2+}]_i$ carried out on MCF-7 cells after silencing of T-type channels with siRNA.

K^+ currents are essential for the maintenance of negative resting membrane potential in most cells, where inhibition of these currents drives the potential toward more depolarized values. Based on these notions, K^+ currents have been proposed to underlie $[Ca^{2+}]_i$ oscillations that occur in a cell cycle-dependent manner in many types of tumor cells. In this model, the activation of T-type Ca^{2+} currents occurs because of membrane potential depolarization induced by a decrease of K^+ channel activity. Cell cycle-dependent kinase activities are thought to inhibit K^+ channel currents, leading to depolarization that could activate T-type Ca^{2+} channels and produce further depolarization by recruiting more Ca^{2+} channels [23].

Our data suggests a similar mechanism for the effect of EGCG on $[Ca^{2+}]_i$ in MCF-7 cells (Fig. 7). We hypothesized this process as follows:

(1) EGCG reduces K^+ currents, possibly acting on Kv1.1 and other K^+ channels, and leads to depolarization that activates T-type Ca^{2+} channels;

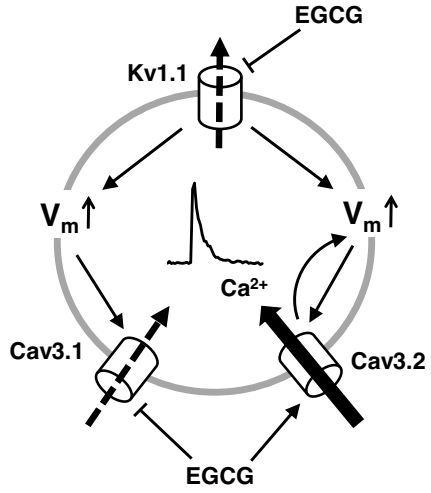

Fig. 7. Diagram showing a possible mechanism of action for the effect of EGCG on $[Ca^{2+}]_i$ (see Section 4 for details).

(2) EGCG selectively enhances the activity of Cav3.2 channels, favoring the onset of an inward Ca^{2+} current and possibly sustaining voltage-driven Cav3.2 cascade recruitment;
(3) this complex of events eventually lead to the observed $[Ca^{2+}]_i$ spike.

The observed EGCG-induced decrease of Cav3.1 activity would not hinder the occurrence of $[Ca^{2+}]_i$ rise in MCF-7 cells, due to the higher relative expression and activation level of Cav3.2. Also, differences in time courses between Ca^{2+} current measurements and $[Ca^{2+}]_i$ confocal imaging can be easily explained by considering that, after $[Ca^{2+}]_i$ rise, baseline recovery operated by Ca^{2+} homeostasis systems is much longer than Ca^{2+} influx dynamics. Moreover, transient calcium entry through T-type calcium channels is likely to lead to long-term Ca^{2+}-induced Ca^{2+} release from internal stores [38].

The inhibition of different kinds of K^+ currents by EGCG has been reported previously [39–41]. However, no data to date has described EGCG actions on T-type Ca^{2+} channels. Our findings show that the EGCG-dependent $[Ca^{2+}]_i$ spike in MCF-7 cells is essentially redox-dependent. Prevention of the $[Ca^{2+}]_i$ spike and reversal of K^+ current inhibition by catalase confirm the occurrence of H_2O_2 release by EGCG in the cell medium in agreement with previous reports [42,43]. Whether the effects of EGCG observed in our experiments depend on a direct action of H_2O_2 on Cav3.2 or other channels, or are the consequence of receptor-mediated effects remains to be established.

Support for both hypotheses can be found in the available literature. Hydrogen peroxide has been found to inhibit voltage-gated K^+ channels in arterial smooth muscle cells, followed by membrane depolarization and Ca^{2+} channel activation [44]. Receptor-dependent effects of EGCG are also well documented. The 67-kDa laminin receptor (67-LR) is considered a major EGCG molecular target in determining the efficacy of EGCG cancer-preventive properties [45,46]. This receptor is expressed in a variety of tumor cells and its expression level strongly correlates with the risk of tumor invasion and metastasis [47,48]. Other signaling pathways possibly targeted by EGCG include the Fas-Fas ligand system, β-catenin-dependent signaling, and the EGFR growth factor receptor, while cross talk between EGCG redox activity and the activation of this latter receptor has also been highlighted [49–51].

Regardless of the mechanism linking EGCG redox properties and its effects on MCF-7 ion currents, our present data are in line with our previous findings in malignant mesothelioma, concerning a redox-dependent EGCG dysregulation of $[Ca^{2+}]_i$ involving Cav3.2 channels [20]. Here we have also shown that Cav3.2 is at least in part responsible for the inhibitory effect of EGCG on MCF-7 cell viability. Hence, the effect of EGCG on $[Ca^{2+}]_i$ seems relevant for the possible use of this green tea polyphenol in the treatment of breast cancer.

In conclusion, this is the first report showing that EGCG affects $[Ca^{2+}]_i$ regulation via ion channel modulation, entailing both Ca^{2+} and K^+ currents. These data open up a new horizon for the use of the green tea polyphenol as a therapeutic tool in the treatment of breast cancer and other malignancies expressing T-type Ca^{2+} channels.

Acknowledgements

This study was supported by Fondazione Buzzi Unicem (Casale Monferrato, Italy), grant n. FBU-P27. Work in the laboratory of T.P. Snutch is supported by an operating grant from the Canadian Institutes of Health Research (#10677) and a Canada Research Chair in Biotechnology and Genomics-Neurobiology. We thank Drs Esperanza Garcia, Elena Borgo and Luca Gatti for their support with experiments.

References

[1] B. Ciapa, D. Pesando, M. Wilding, M. Whitaker, Cell-cycle calcium transients driven by cyclic changes in inositol trisphosphate levels, Nature 368 (1994) 875–878.
[2] D.E. Clapham, Calcium signaling, Cell 131 (2007) 1047–1058.
[3] S. Orrenius, B. Zhivotovsky, P. Nicotera, Regulation of cell death: the calcium-apoptosis link, Nat. Rev. Mol. Cell Biol. 4 (2003) 552–565.
[4] J. Parkash, K. Asotra, Calcium wave signaling in cancer cells, Life Sci. 87 (2010) 587–595.
[5] G.R. Monteith, D. McAndrew, H.M. Faddy, S.J. Roberts-Thomson, Calcium and cancer: targeting Ca^{2+} transport, Nat. Rev. Cancer 7 (2007) 519–530.
[6] D.J. Triggle, Calcium channel antagonists: clinical uses – past, present and future, Biochem. Pharmacol. 74 (2007) 1–9.
[7] L. Chen, H.Y. Zhang, Cancer preventive mechanisms of the green tea polyphenol (−)-epigallocatechin-3-gallate, Molecules 12 (2007) 946–957.
[8] S. Shankar, S. Ganapathy, R.K. Srivastava, Green tea polyphenols: biology and therapeutic implications in cancer, Front. Biosci. 12 (2007) 4881–4899.
[9] Z.P. Chen, J.B. Schell, C.T. Ho, K.Y. Chen, Green tea epigallocatechin gallate shows a pronounced growth inhibitory effect on cancerous cells but not on their normal counterparts, Cancer Lett. 129 (1998) 173–179.
[10] A.R. Amin, F.R. Khuri, Z.G. Chen, D.M. Shin, Synergistic growth inhibition of squamous cell carcinoma of the head and neck by erlotinib and epigallocatechin-3-gallate: the role of p53-dependent inhibition of nuclear factor-kappaB, Cancer Prev. Res. (Phila.) 2 (2009) 538–545.
[11] M.E. Stearns, M. Wang, Synergistic effects of the green tea extract epigallocatechin-3-gallate and taxane in eradication of malignant human prostate tumors, Transl. Oncol. 4 (2011) 147–156.
[12] H. Wu, Y. Xin, C. Xu, Y. Xiao, Capecitabine combined with (−)-epigallocatechin-3-gallate inhibits angiogenesis and tumor growth in nude mice with gastric cancer xenografts, Exp. Ther. Med. 3 (2012) 650–654.
[13] N.M. Yunos, P. Beale, J.Q. Yu, F. Huq, Synergism from sequenced combinations of curcumin and epigallocatechin-3-gallate with cisplatin in the killing of human ovarian cancer cells, Anticancer Res. 31 (2011) 1131–1140.
[14] V. Volta, E. Ranzato, S. Martinotti, S. Gallo, M.V. Russo, L. Mutti, S. Biffo, B. Burlando, Preclinical demonstration of synergistic active nutrients/drug (AND) combination as a potential treatment for malignant pleural mesothelioma, PLOS ONE 8 (2013) e58051.
[15] A.H. Wu, M.C. Yu, Tea, hormone-related cancers and endogenous hormone levels, Mol. Nutr. Food Res. 50 (2006) 160–169.
[16] E.C. Stuart, M.J. Scandlyn, R.J. Rosengren, Role of epigallocatechin gallate (EGCG) in the treatment of breast and prostate cancer, Life Sci. 79 (2006) 2329–2336.
[17] E. Alvarez-Castro, M. Campos-Toimil, F. Orallo, (−)-Epigallocatechin-3-gallate induces contraction of the rat aorta by a calcium influx-dependent mechanism, Naunyn Schmiedebergs Arch. Pharmacol. 369 (2004) 496–506.
[18] H.J. Kim, K.S. Yum, J.H. Sung, D.J. Rhie, M.J. Kim, D.S. Min, S.J. Hahn, M.S. Kim, Y.H. Jo, S.H. Yoon, Epigallocatechin-3-gallate increases intracellular $[Ca^{2+}]$ in U87 cells mainly by influx of extracellular Ca^{2+} and partly by release of intracellular stores, Naunyn Schmiedebergs Arch. Pharmacol. 369 (2004) 260–267.
[19] S.T. Yin, M.L. Tang, H.M. Deng, T.R. Xing, J.T. Chen, H.L. Wang, D.Y. Ruan, Epigallocatechin-3-gallate induced primary cultures of rat hippocampal neurons death linked to calcium overload and oxidative stress, Naunyn Schmiedebergs Arch. Pharmacol. 379 (2009) 551–564.
[20] E. Ranzato, S. Martinotti, V. Magnelli, B. Murer, S. Biffo, L. Mutti, B. Burlando, Epigallocatechin-3-gallate induces mesothelioma cell death via

H_2O_2-dependent T-type Ca^{2+} channel opening, J. Cell Mol. Med. 16 (2012) 2667–2678.
[21] Y. Zhang, X. Jiang, T.P. Snutch, J. Tao, Modulation of low-voltage-activated T-type Ca(2+) channels, Biochim. Biophys. Acta 1828 (2012) 1550–1559.
[22] J.T. Taylor, X.B. Zeng, J.E. Pottle, K. Lee, A.R. Wang, S.G. Yi, J.A. Scruggs, S.S. Sikka, M. Li, Calcium signaling and T-type calcium channels in cancer cell cycling, World J. Gastroenterol. 14 (2008) 4984–4991.
[23] A. Panner, R.D. Wurster, T-type calcium channels and tumor proliferation, Cell Calcium 40 (2006) 253–259.
[24] H.D. Soule, J. Vazguez, A. Long, S. Albert, M. Brennan, A human cell line from a pleural effusion derived from a breast carcinoma, J. Natl. Cancer Inst. 51 (1973) 1409–1416.
[25] T. Ohkubo, J. Yamazaki, T-type voltage-activated calcium channel Cav3.1, but not Cav3.2, is involved in the inhibition of proliferation and apoptosis in MCF-7 human breast cancer cells, Int. J. Oncol. 41 (2012) 267–275.
[26] J.T. Taylor, L. Huang, J.E. Pottle, K. Liu, Y. Yang, X. Zeng, B.M. Keyser, K.C. Agrawal, J.B. Hansen, M. Li, Selective blockade of T-type Ca^{2+} channels suppresses human breast cancer cell proliferation, Cancer Lett. 267 (2008) 116–124.
[27] G.E. Bertolesi, C. Shi, L. Elbaum, C. Jollimore, G. Rozenberg, S. Barnes, M.E. Kelly, The Ca(2+) channel antagonists mibefradil and pimozide inhibit cell growth via different cytotoxic mechanisms, Mol. Pharmacol. 62 (2002) 210–219.
[28] E. Tringham, K.L. Powell, S.M. Cain, K. Kuplast, J. Mezeyova, M. Weerapura, C. Eduljee, X. Jiang, P. Smith, J.L. Morrison, N.C. Jones, E. Braine, G. Rind, M. Fee-Maki, D. Parker, H. Pajouhesh, M. Parmar, T.J. O'Brien, T.P. Snutch, T-type calcium channel blockers that attenuate thalamic burst firing and suppress absence seizures, Sci. Transl. Med. 4 (2012) 121ra19.
[29] G. Grynkiewicz, M. Poenie, R.Y. Tsien, A new generation of Ca^{2+} indicators with greatly improved fluorescence properties, J. Biol. Chem. 260 (1985) 3440–3450.
[30] C. Marchetti, P. Gavazzo, Subunit-dependent effects of nickel on NMDA receptor channels, Brain Res. Mol. Brain Res. 117 (2003) 139–144.
[31] F. Belardetti, E. Tringham, C. Eduljee, X. Jiang, H. Dong, A. Hendricson, Y. Shimizu, D.L. Janke, D. Parker, J. Mezeyova, A. Khawaja, H. Pajouhesh, R.A. Fraser, S.P. Arneric, T.P. Snutch, A fluorescence-based high-throughput screening assay for the identification of T-type calcium channel blockers, Assay Drug Dev. Technol. 7 (2009) 266–280.
[32] M. Barnes, R. Correll, D. Stevens, A simple spreadsheet for estimating low-effect concentrations and associated logistic dose response curves, in: A.P.A.S.o.E. The Society of Environmental Toxicology and Chemistry (Ed.), Solutions to Pollution: Program Abstract Book, SETAC ASE Asia Pacific, 2003.
[33] E. Donnadieu, G. Bismuth, A. Trautmann, Calcium fluxes in T lymphocytes, J. Biol. Chem. 267 (1992) 25864–25872.
[34] L.S. Gray, E. Perez-Reyes, J.C. Gomora, D.M. Haverstick, M. Shattock, L. McLatchie, J. Harper, G. Brooks, T. Heady, T.L. Macdonald, The role of voltage gated T-type Ca^{2+} channel isoforms in mediating capacitative Ca^{2+} entry in cancer cells, Cell Calcium 36 (2004) 489–497.
[35] H. Ouadid-Ahidouch, F. Chaussade, M. Roudbaraki, C. Slomianny, E. Dewailly, P. Delcourt, N. Prevarskaya, KV1.1 K(+) channels identification in human breast carcinoma cells: involvement in cell proliferation, Biochem. Biophys. Res. Commun. 278 (2000) 272–277.
[36] Y.D. Hsuuw, W.H. Chan, Epigallocatechin gallate dose-dependently induces apoptosis or necrosis in human MCF-7 cells, Ann. N. Y. Acad. Sci. 1095 (2007) 428–440.
[37] W. Li, S.L. Zhang, N. Wang, B.B. Zhang, M. Li, Blockade of T-type Ca(2+) channels inhibits human ovarian cancer cell proliferation, Cancer Invest. 29 (2011) 339–346.
[38] R.T. Morton-Jones, M.B. Cannell, G.D. Housley, Ca^{2+} entry via AMPA-type glutamate receptors triggers Ca^{2+}-induced Ca^{2+} release from ryanodine receptors in rat spiral ganglion neurons, Cell Calcium 43 (2008) 356–366.
[39] H.S. Jeong, S. Jang, M.J. Jang, S.G. Lee, T.S. Kim, H. Tag, J.H. Lee, J.Y. Jun, J.S. Park, Effects of (−)-epigallocatechin-3-gallate on the activity of substantia nigra dopaminergic neurons, Brain Res. 1130 (2007) 114–118.
[40] B.H. Choi, J.S. Choi, D.S. Min, S.H. Yoon, D.J. Rhie, Y.H. Jo, M.S. Kim, S.J. Hahn, Effects of (−)-epigallocatechin-3-gallate, the main component of green tea, on the cloned rat brain Kv1.5 potassium channels, Biochem. Pharmacol. 62 (2001) 527–535.
[41] H.S. Jeong, Y.S. Kim, J.S. Park, Modulation of neuronal activity by EGCG, Brain Res. 1047 (2005) 267–270.
[42] L. Elbling, R.M. Weiss, O. Teufelhofer, M. Uhl, S. Knasmueller, R. Schulte-Hermann, W. Berger, M. Micksche, Green tea extract and (−)-epigallocatechin-3-gallate, the major tea catechin, exert oxidant but lack antioxidant activities, FASEB J. 19 (2005) 807–809.
[43] M.M. Chan, K.J. Soprano, K. Weinstein, D. Fong, Epigallocatechin-3-gallate delivers hydrogen peroxide to induce death of ovarian cancer cells and enhances their cisplatin susceptibility, J. Cell Physiol. 207 (2006) 389–396.
[44] S.L. Archer, X.C. Wu, B. Thebaud, R. Moudgil, K. Hashimoto, E.D. Michelakis, O_2 sensing in the human ductus arteriosus: redox-sensitive K^+ channels are regulated by mitochondria-derived hydrogen peroxide, Biol. Chem. 385 (2004) 205–216.
[45] D. Umeda, S. Yano, K. Yamada, H. Tachibana, Green tea polyphenol epigallocatechin-3-gallate signaling pathway through 67-kDa laminin receptor, J. Biol. Chem. 283 (2008) 3050–3058.
[46] Y. Fujimura, M. Sumida, K. Sugihara, S. Tsukamoto, K. Yamada, H. Tachibana, Green tea polyphenol EGCG sensing motif on the 67-kDa laminin receptor, PLOS ONE 7 (2012) e37942.
[47] S. Martignone, S. Menard, R. Bufalino, N. Cascinelli, R. Pellegrini, E. Tagliabue, S. Andreola, F. Rilke, M.I. Colnaghi, Prognostic significance of the 67-kilodalton laminin receptor expression in human breast carcinomas, J. Natl. Cancer Inst. 85 (1993) 398–402.
[48] S. Menard, V. Castronovo, E. Tagliabue, M.E. Sobel, New insights into the metastasis-associated 67 kD laminin receptor, J. Cell Biochem. 67 (1997) 155–165.
[49] Z. Hou, S. Sang, H. You, M.J. Lee, J. Hong, K.V. Chin, C.S. Yang, Mechanism of action of (−)-epigallocatechin-3-gallate: auto-oxidation-dependent inactivation of epidermal growth factor receptor and direct effects on growth inhibition in human esophageal cancer KYSE 150 cells, Cancer Res. 65 (2005) 8049–8056.
[50] H.Y. Lin, S.C. Hou, S.C. Chen, M.C. Kao, C.C. Yu, S. Funayama, C.T. Ho, T.D. Way, (−)-Epigallocatechin gallate induces Fas/CD95-mediated apoptosis through inhibiting constitutive and IL-6-induced JAK/STAT3 signaling in head and neck squamous cell carcinoma cells, J. Agric. Food Chem. 60 (2012) 2480–2489.
[51] T. Singh, S.K. Katiyar, Green tea polyphenol, (−)-epigallocatechin-3-gallate, induces toxicity in human skin cancer cells by targeting beta-catenin signaling, Toxicol. Appl. Pharmacol. 273 (2013) 418–424.